Prediction of Respiration-Induced Internal 3-D Deformation Fields From Dense External 3-D Surface Motion

Oliver Taubmann[1,2], Jakob Wasza[1], Christoph Forman[1,2], Peter Fischer[1,2], Jens Wetzl[1,2], Andreas Maier[1,2], Joachim Hornegger[1,2]

June 26, 2014 – CARS, Fukuoka, Japan

[1] Pattern Recognition Lab, FAU Erlangen-Nuremberg, Germany
[2] Erlangen Graduate School in Advanced Optical Technologies (SAOT)

FRIEDRICH-ALEXANDER UNIVERSITÄT ERLANGEN-NÜRNBERG
TECHNISCHE FAKULTÄT

Outline

Motivation

- Procedures in thorax/abdomen benefit from respiratory motion compensation (radiation therapy, cardiac interventions, . . .)
- Intraprocedural tracking of *dense* internal motion is not feasible

Approach:

- Employ external surrogate for internal motion prediction
- E.g. phase/amplitude information from spirometry or point tracking $\Rightarrow$ typically low-dim. surrogates

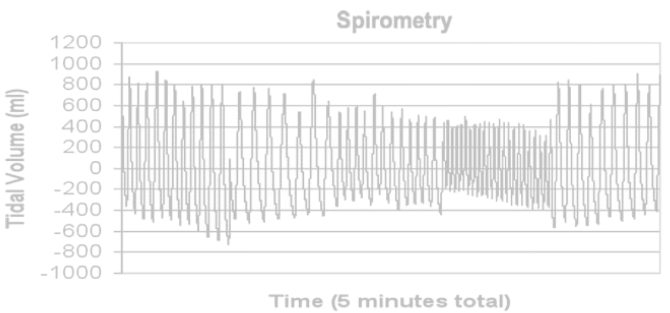

Figure: Respiratory surrogate acquired with a spirometer, from [Hughes et al., 2009].

Motivation

- Procedures in thorax/abdomen benefit from respiratory motion compensation (radiation therapy, cardiac interventions, . . .)
- Intraprocedural tracking of *dense* internal motion is not feasible

Approach:

- Employ external surrogate for internal motion prediction
- E.g. phase/amplitude information from spirometry or point tracking
  $\Rightarrow$ typically low-dim. surrogates

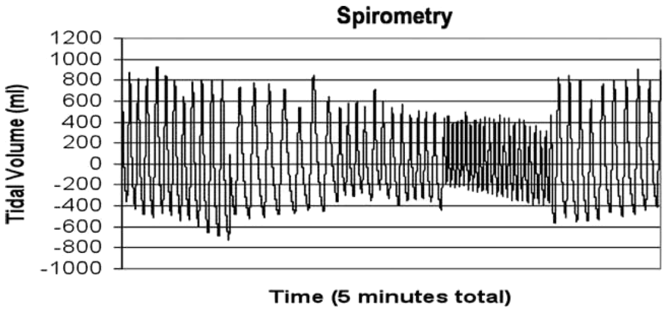

Figure: Respiratory surrogate acquired with a spirometer, from [Hughes et al., 2009].

Motivation (cont.)

Challenges:

- *Intra-cycle* variation – in-/exhalation (“hysteresis”)
- *Inter-cycle* variation – abdominal/thoracic breathing (“reproducibility”)
- *Inter-subject* variation

$\Rightarrow$ More sophisticated, higher-dimensional surrogates

Idea: Use the whole body surface

- Increasing affordability of real-time range imaging (RI)
- Markerless and non-intrusive acquisition
- Better correlation [Fayad et al., 2012, Hughes et al., 2009]

Motivation (cont.)

Challenges:

- *Intra-cycle* variation – in-/exhalation (“hysteresis”)
- *Inter-cycle* variation – abdominal/thoracic breathing (“reproducibility”)
- *Inter-subject* variation

$\Rightarrow$ More sophisticated, higher-dimensional surrogates

Idea: Use the whole body surface

- Increasing affordability of real-time range imaging (RI)
- Markerless and non-intrusive acquisition
- Better correlation [Fayad et al., 2012, Hughes et al., 2009]

Contributions

Statistical prediction framework making use of the whole surface

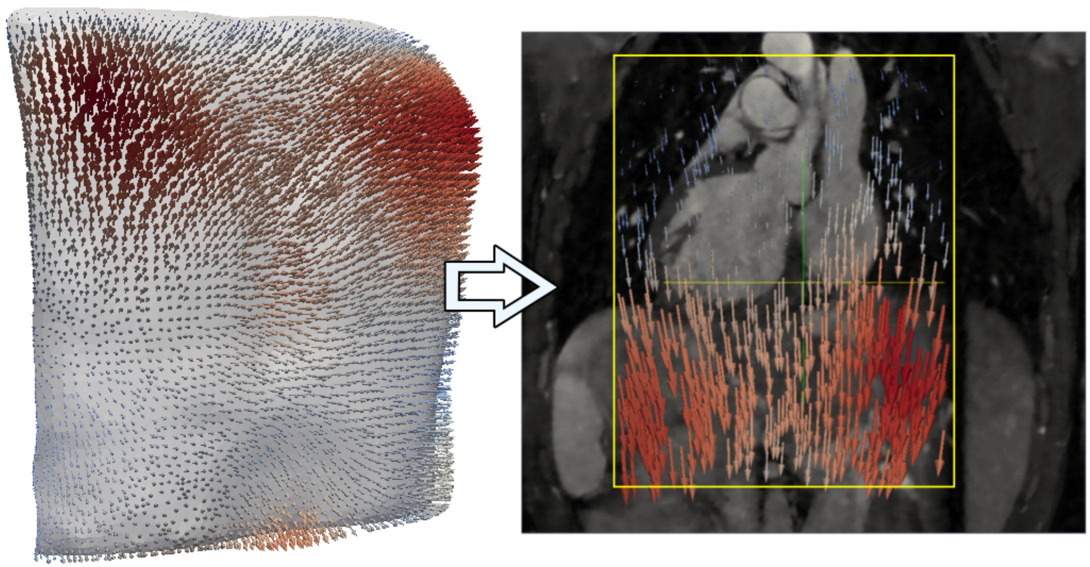

- Dense 3-D motion fields both internally and externally
- Comprehensive study of several parameters (smoothness, coverage, ...)

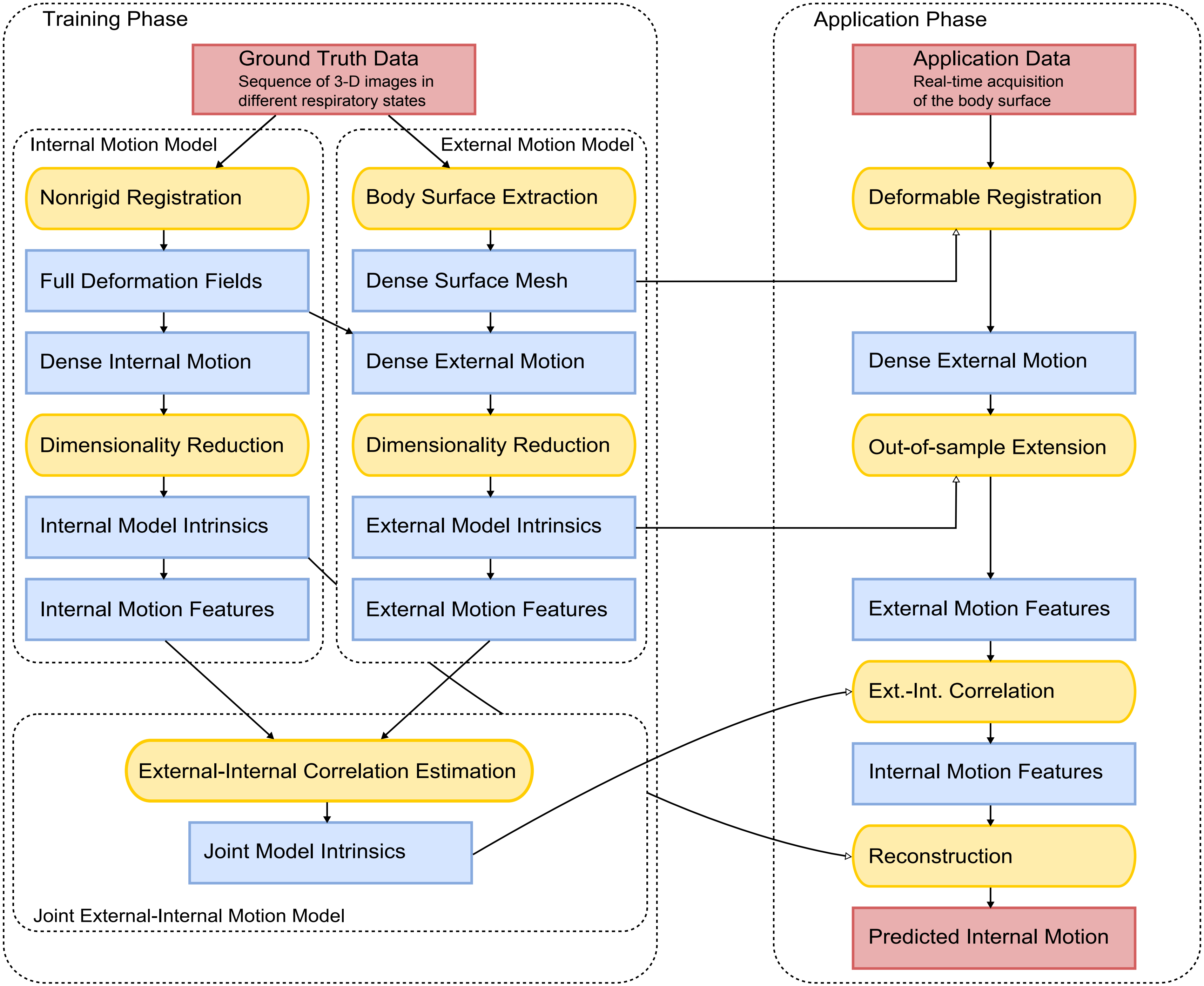

Training Phase
Ground Truth Data
Sequence of 3-D images in
different respiratory states
Internal Motion Model
External Motion Model
Nonrigid Registration
Body Surface Extraction
Full Deformation Fields
Dense Surface Mesh
Dense Internal Motion
Dense External Motion
Dimensionality Reduction
Dimensionality Reduction
Internal Model Intrinsics
External Model Intrinsics
Internal Motion Features
External Motion Features
External-Internal Correlation Estimation
Joint Model Intrinsics
Joint External-Internal Motion Model
Application Phase
Application Data
Real-time acquisition
of the body surface
Deformable Registration
Dense External Motion
Out-of-sample Extension
External Motion Features
Ext.-Int. Correlation
Internal Motion Features
Reconstruction
Predicted Internal Motion

Respiratory Motion Modeling

Internal Motion Model

External Motion Model

Joint Motion Model

FRIEDRICH-ALEXANDER
UNIVERSITÄT
ERLANGEN-NÜRNBERG

TECHNISCHE FAKULTÄT

Nonrigid Volumetric Registration

Curvature-regularized framework [Fischer and Modersitzki, 2004], deformation field $\boldsymbol{D}^*$ minimizes the functional

$$\mathcal{J}[\boldsymbol{D}] = \mathcal{U}[\boldsymbol{R}, \boldsymbol{T}; \boldsymbol{D}] + \alpha\mathcal{S}^{\text{curv}}[\boldsymbol{D}]. \tag{1}$$

$\boldsymbol{R}, \boldsymbol{T}$	Reference and template volumes
$\mathcal{U}$	Distance measure, in our case implied by Demons [Thirion, 1995]
$\alpha\mathcal{S}^{\text{curv}}$	Penalizes high curvatures, α controls degree of regularization

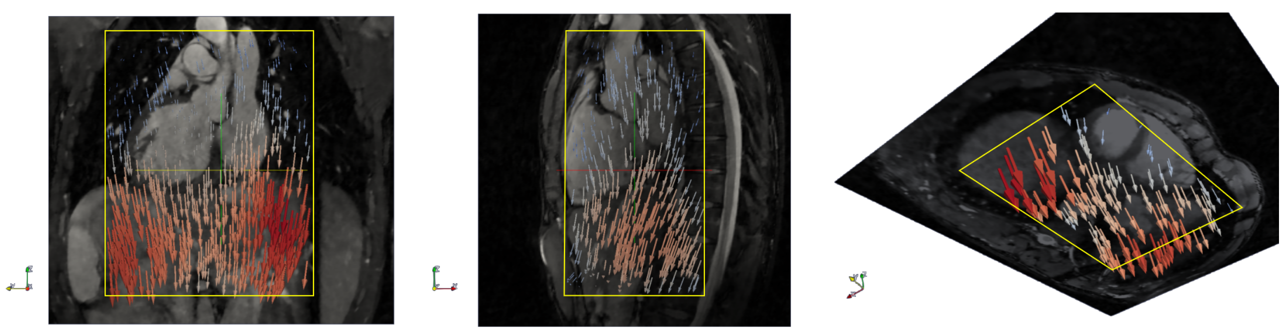

Figure: Respiratory motion field cropped to an internal ROI.

Model Intrinsics

Perform *invertible* dimensionality reduction on data matrix:

$$\boldsymbol{Y} = [\tilde{\boldsymbol{d}}_0^{\text{int}}, \ldots, \tilde{\boldsymbol{d}}_{t_{\text{ref}}-1}^{\text{int}}, \tilde{\boldsymbol{d}}_{t_{\text{ref}}+1}^{\text{int}}, \ldots, \tilde{\boldsymbol{d}}_N^{\text{int}}]^\top \in \mathbb{R}^{N \times 3M} \tag{2}$$

$\tilde{\boldsymbol{d}}_t^{\text{int}}$	Mean-centered internal deformation fields (vectorized)
N	Number of deformation fields
M	Number of vectors per field

- Compute first r principal components $\boldsymbol{v}_i$,

$$\boldsymbol{Q} = [\boldsymbol{v}_0, \boldsymbol{v}_1, \ldots, \boldsymbol{v}_{r-1}] \in \mathbb{R}^{3M \times r}, \tag{3}$$

- and projections onto them (mapped, r-dim. points) as features,

$$\boldsymbol{Y}_m = \boldsymbol{Y}\boldsymbol{Q} \tag{4}$$

Respiratory Motion Modeling

Internal Motion Model

External Motion Model

Joint Motion Model

Surface Extraction

- Acquisition using RI system combined with MRI is difficult (limited room inside scanner, electromagnetic interference, . . .)

  $\Rightarrow$ Extract surface and its motion directly from volumetric data

- Ray-casting based approach to extraction
- Cylindrical sensor avoids shortcomings of pinhole camera model

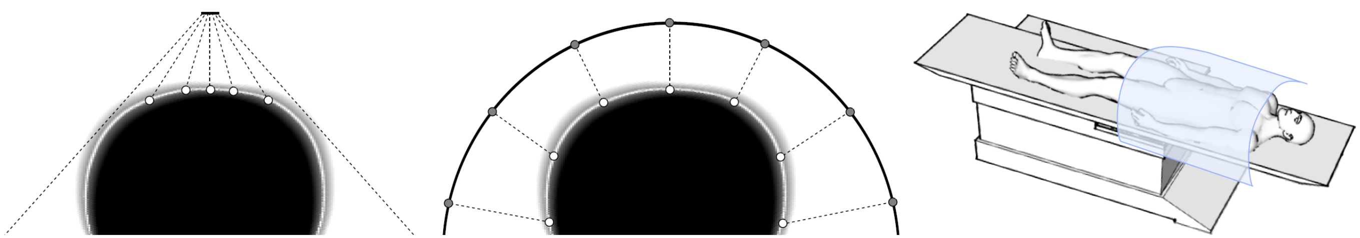

Figure: Virtual sensor geometries. Left and middle images adapted from [Wasza et al., 2013].

Model Intrinsics

Perform *extensible* dimensionality reduction on data matrix:

$$\boldsymbol{X} = [\tilde{\boldsymbol{d}}_0^{\text{ext}}, \dots, \tilde{\boldsymbol{d}}_{t_{\text{ref}}-1}^{\text{ext}}, \tilde{\boldsymbol{d}}_{t_{\text{ref}}+1}^{\text{ext}}, \dots, \tilde{\boldsymbol{d}}_N^{\text{ext}}]^\top \in \mathbb{R}^{N \times 3V} \quad (5)$$

$\tilde{\boldsymbol{d}}_t^{\text{ext}}$	Mean-centered external deformation fields (vectorized)
N	Number of deformation fields
V	Number of surface vertices / motion vectors

- Generate features $\boldsymbol{X}_m \in \mathbb{R}^{N \times l}$ as before with PCA, or…

Model Intrinsics (cont.)

- . . . alternatively, use a nonlinear method, such as:

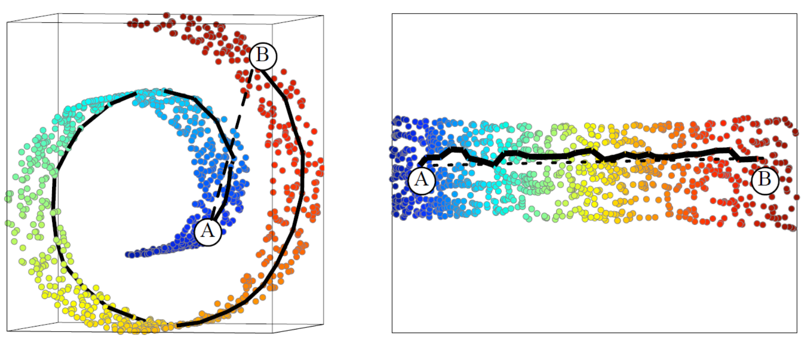

Image source: [Saul et al., 2006]

Isomap
[Tenenbaum et al., 2000]

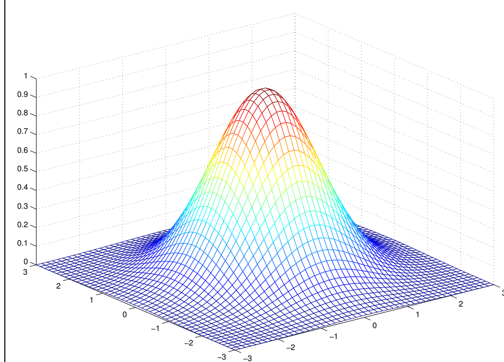

$$k(\boldsymbol{x}_1, \boldsymbol{x}_2) = \exp\left(\frac{-||\boldsymbol{x}_1 - \boldsymbol{x}_2||_2^2}{2\sigma^2}\right)$$

Kernel PCA (Gaussian RBF)
[Schölkopf et al., 1998]

Respiratory Motion Modeling

Internal Motion Model

External Motion Model

Joint Motion Model

FRIEDRICH-ALEXANDER
UNIVERSITÄT
ERLANGEN-NÜRNBERG
TECHNISCHE FAKULTÄT

External-Internal Correlation

- Correlate feature spaces with a simple regression, complexity should be handled by individual models

- We use multivariate multilinear regression (cf. [Klinder et al., 2010]):

$$\boldsymbol{B} = \underset{\boldsymbol{B}'}{\operatorname{argmin}}\, \operatorname{tr}\left[\left(\boldsymbol{Y}_m - \boldsymbol{X}_m\boldsymbol{B}'^\top\right)\left(\boldsymbol{Y}_m - \boldsymbol{X}_m\boldsymbol{B}'^\top\right)^\top\right], \tag{6}$$

where $\boldsymbol{B} \in \mathbb{R}^{r\times l}$ is the ordinary least squares estimator for $\boldsymbol{Y}_m = \boldsymbol{X}_m\boldsymbol{B}^\top$.

Experiments and Results

FRIEDRICH-ALEXANDER
UNIVERSITÄT
ERLANGEN-NÜRNBERG
TECHNISCHE FAKULTÄT

Data

Synthetic Data

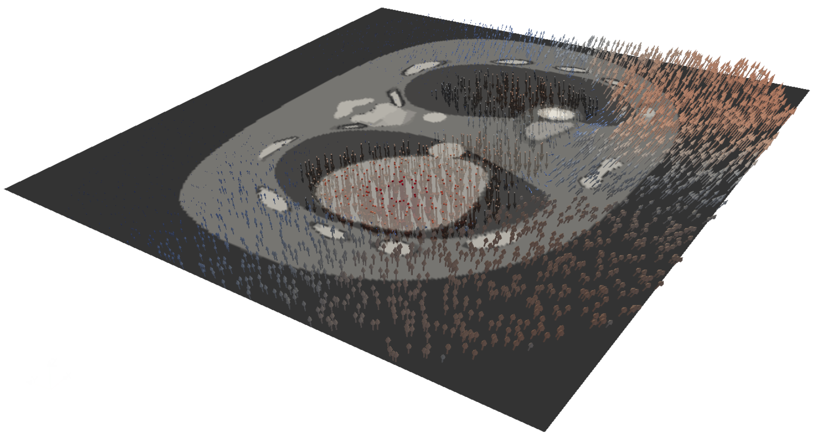

Derived from XCAT phantom
[Segars et al., 2010,
Maier et al., 2014]

Volunteer Data

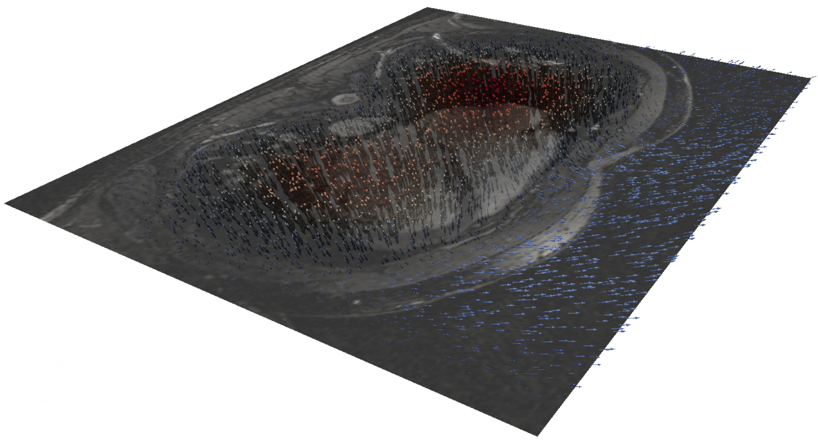

Time-resolved cardiac MRI
of 6 healthy volunteers
[Forman et al., 2013]

Experimental Setup

- Test phase distant from reference, but not full ex-/inhale
- Exclude adjacent phases from training to reduce bias
- Error: Vector magnitudes of difference,

$$\left\{ \left\| \boldsymbol{D}_{\text{predicted}}(x_i, y_i, z_i) - \boldsymbol{D}_{\text{ground truth}}(x_i, y_i, z_i) \right\|_2 \right\}_{i=1\ldots M} \tag{7}$$

- Magnitudes of internal displacements in test phase:

ID	Magnitude [mm]	ID	Magnitude [mm]
P1	3.53 ± 1.81	P2	3.87 ± 1.66
P3	3.26 ± 1.45	P4	4.56 ± 1.70
P5	1.99 ± 0.61	P6	0.43 ± 0.17
XCAT	3.51 ± 3.62		

Experimental Setup

- Test phase distant from reference, but not full ex-/inhale
- Exclude adjacent phases from training to reduce bias

- Error: Vector magnitudes of difference,

$$\{\|\boldsymbol{D}_{\text{predicted}}(x_i, y_i, z_i) - \boldsymbol{D}_{\text{ground truth}}(x_i, y_i, z_i)\|_2\}_{i=1\ldots M} \tag{7}$$

- Magnitudes of internal displacements in test phase:

ID	Magnitude [mm]	ID	Magnitude [mm]
P1	3.53 ± 1.81	P2	3.87 ± 1.66
P3	3.26 ± 1.45	P4	4.56 ± 1.70
P5	1.99 ± 0.61	P6	0.43 ± 0.17
XCAT	3.51 ± 3.62		

Experimental Setup

- Test phase distant from reference, but not full ex-/inhale
- Exclude adjacent phases from training to reduce bias
- Error: Vector magnitudes of difference,

$$\{\|\boldsymbol{D}_{\text{predicted}}(x_i, y_i, z_i) - \boldsymbol{D}_{\text{ground truth}}(x_i, y_i, z_i)\|_2\}_{i=1\ldots M} \quad (7)$$

- Magnitudes of internal displacements in test phase:

ID	Magnitude [mm]	ID	Magnitude [mm]
P1	3.53 ± 1.81	P2	3.87 ± 1.66
P3	3.26 ± 1.45	P4	4.56 ± 1.70
P5	1.99 ± 0.61	P6	0.43 ± 0.17
XCAT	3.51 ± 3.62		

Results – Surface Coverage

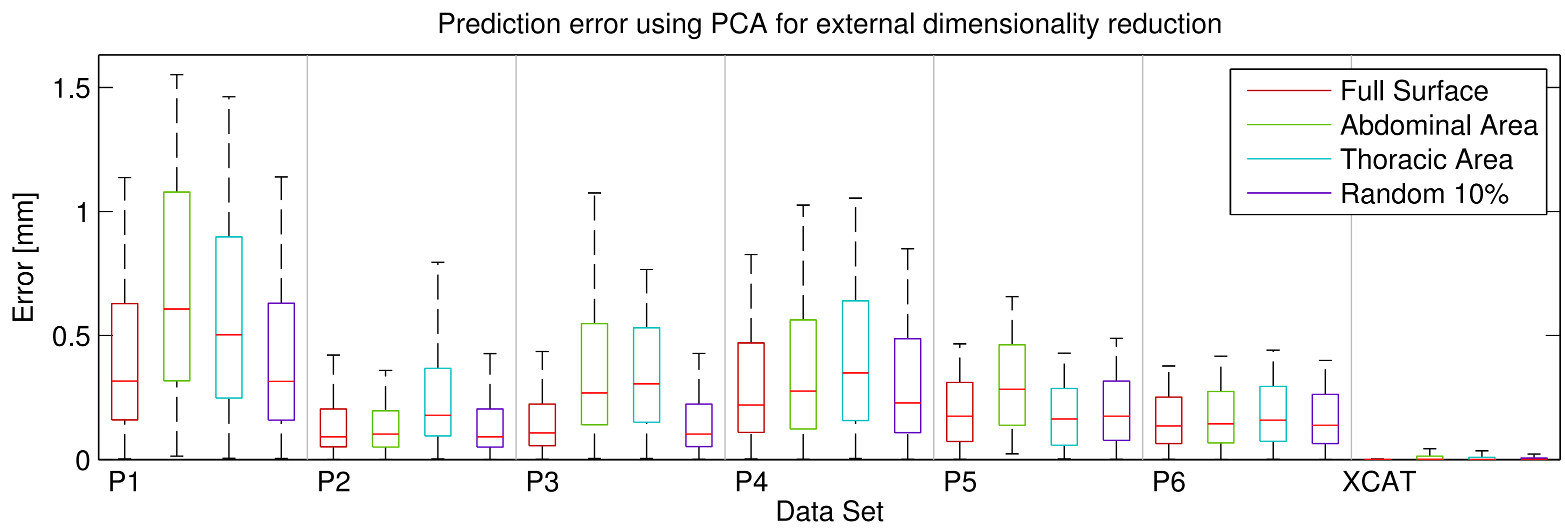

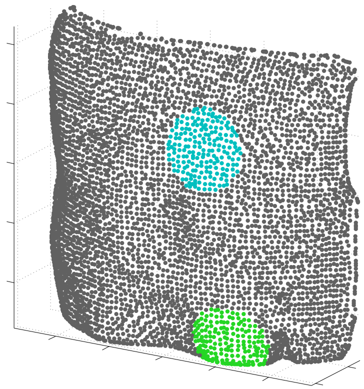

- Small thoracic/abdominal areas consistently yield equal or worse results
- With large coverage, uniformly distributed random 10% are sufficient

Results – Smoothness of Registration

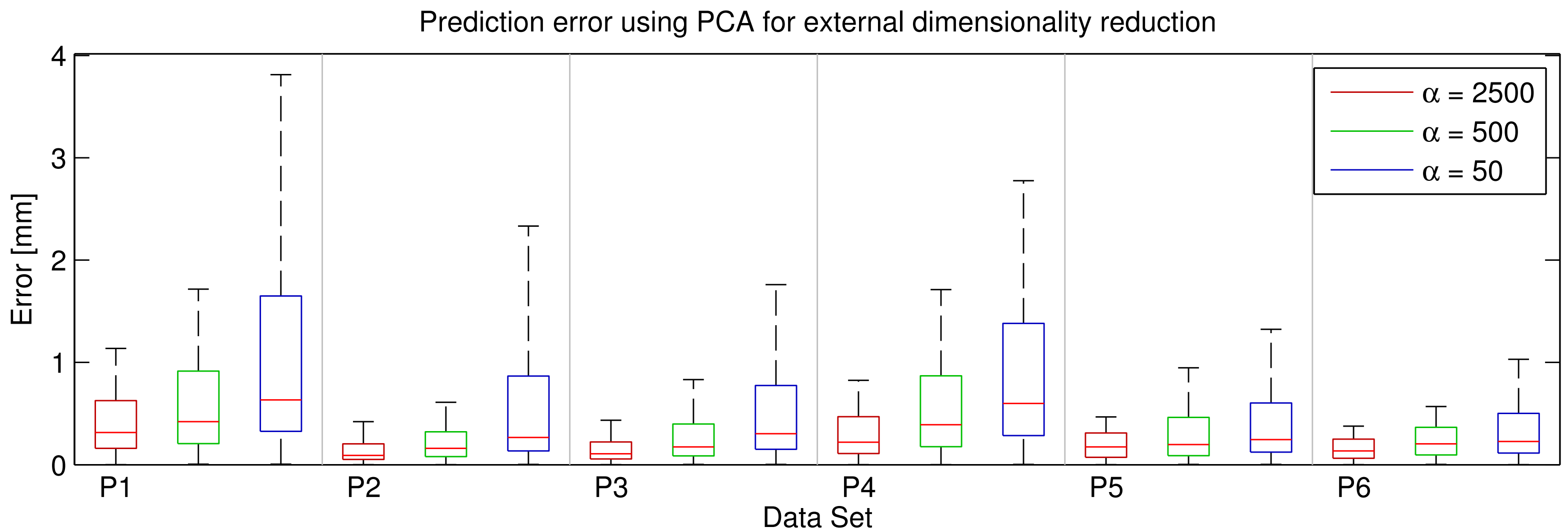

- Motivation: “accuracy” ↔ “anatomical plausibility”
- Weaker regularization results in more complex/noisy motion fields that are harder to predict accurately

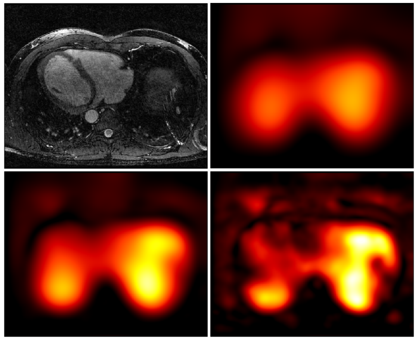

Summary and Outlook

- Prediction framework with promising accuracy
- *Dense* internal displacements from *dense* external surface motion

- Evaluated effects of feature dim., coverage, smoothness
- Validated on synthetic 4-D phantom and cardiac MRI of volunteers

- Future work will need to focus on a clinical setting with actual RI

Summary and Outlook

- Prediction framework with promising accuracy
- *Dense* internal displacements from *dense* external surface motion

- Evaluated effects of feature dim., coverage, smoothness
- Validated on synthetic 4-D phantom and cardiac MRI of volunteers

- Future work will need to focus on a clinical setting with actual RI

Summary and Outlook

- Prediction framework with promising accuracy
- *Dense* internal displacements from *dense* external surface motion

- Evaluated effects of feature dim., coverage, smoothness
- Validated on synthetic 4-D phantom and cardiac MRI of volunteers

- Future work will need to focus on a clinical setting with actual RI

Summary and Outlook

- Prediction framework with promising accuracy
- *Dense* internal displacements from *dense* external surface motion

- Evaluated effects of feature dim., coverage, smoothness
- Validated on synthetic 4-D phantom and cardiac MRI of volunteers

- Future work will need to focus on a clinical setting with actual RI

Any questions?

Thanks for your attention!

References

Bauer, S., Berkels, B., Ettl, S., Arold, O., Hornegger, J., and Rumpf, M. (2012).
Marker-less Reconstruction of Dense 4-D Surface Motion Fields using Active Laser Triangulation for Respiratory Motion Management.
In Ayache, N., Delingette, H., Golland, P., and Mori, K., editors, *Medical Image Computing and Computer-Assisted Intervention MICCAI 2012*, Lecture Notes in Computer Science, pages 414–421. Springer.

Bengio, Y., Paiement, J.-F., and Vincent, P. (2003).
Out-of-Sample Extensions for LLE, Isomap, MDS, Eigenmaps, and Spectral Clustering.
In *Advances in Neural Information Processing Systems*.

Fayad, H., Pan, T., Pradier, O., and Visvikis, D. (2012).
Patient specific respiratory motion modeling using a 3D patient's external surface.
Med Phys, 39:3386–3395.

Fischer, B. and Modersitzki, J. (2004).
A unified approach to fast image registration and a new curvature based registration technique.
Linear Algebra and its Applications, 380:107–124.

Forman, C., Grimm, R., Hutter, J. M., Maier, A., Hornegger, J., and Zenge, M. O. (2013).
Free-breathing whole-heart coronary MRA: Motion compensation integrated into 3D cartesian compressed sensing reconstruction.
In Mori, K., Sakuma, I., Sato, Y., Barillot, C., and Navab, N., editors, *Medical Image Computing and Computer-Assisted Intervention MICCAI 2013*, Lecture Notes in Computer Science, pages 575–582. Springer.

He, T., Xue, Z., Xie, W., and Wong, S. T. (2010).
Online 4-D CT estimation for patient-specific respiratory motion based on real-time breathing signals.
In Jiang, T., Navab, N., Pluim, J. P., and Viergever, M. A., editors, *Medical Image Computing and Computer-Assisted Intervention MICCAI 2010*, Lecture Notes in Computer Science, pages 392–399. Springer.

References (cont.)

Hughes, S., McClelland, J., Tarte, S., Lawrence, D., Ahmad, S., Hawkes, D., and Landau, D. (2009).
Assessment of two novel ventilatory surrogates for use in the delivery of gated/tracked radiotherapy for non-small cell lung cancer.
Radiotherapy and Oncology, 91:336–341.

Klinder, T., Lorenz, C., and Ostermann, J. (2010).
Prediction framework for statistical respiratory motion modeling.
In *International conference on Medical image computing and computer-assisted intervention*, pages 327–334. Springer.

Maier, A., Taubmann, O., Wetzl, J., Wasza, J., Forman, C., Fischer, P., Hornegger, J., and Fahrig, R. (2014).
Fast Interpolation of Dense Motion Fields from Synthetic Phantoms.
In Deserno, T., Handels, H., Meinzer, H.-P., and Tolxdorff, T., editors, *Bildverarbeitung für die Medizin 2014*, pages 168–173, Berlin.

Saul, L. K., Weinberger, K. Q., Ham, J. H., Sha, F., and Lee, D. D. (2006).
Spectral methods for dimensionality reduction.
Semisupervised Learning. MIT Press: Cambridge, MA.

Schaerer, J., Fassi, A., Riboldi, M., Cerveri, P., Baroni, G., and Sarrut, D. (2012).
Multi-dimensional respiratory motion tracking from markerless optical surface imaging based on deformable mesh registration.
Phys Med Biol, 57:357–373.

Schölkopf, B., Smola, A., and Müller, K.-R. (1998).
Nonlinear component analysis as a kernel eigenvalue problem.
Neural Comput, 10:1299–1319.

References (cont.)

- Segars, W. P., Sturgeon, G., Mendonca, S., Grimes, J., and Tsui, B. M. W. (2010).
  4D XCAT phantom for multimodality imaging research.
  Med Phys, 37:4902–4915.
- Tenenbaum, J. B., de Silva, V., and Langford, J. C. (2000).
  A global geometric framework for nonlinear dimensionality reduction.
  Science, 290:2319–2323.
- Thirion, J.-P. (1995).
  Fast Non-Rigid Matching of 3D Medical Images.
  Technical Report RR-2547, INRIA.
- Wasza, J., Bauer, S., and Hornegger, J. (2012).
  Real-time motion compensated patient positioning and non-rigid deformation estimation using 4-D shape priors.
  MICCAI: International Conference on Medical Image Computing and Computer-Assisted Intervention, 15(Pt 2):576–83.
- Wasza, J., Bauer, S., and Hornegger, J. (2013).
  Real-time respiratory motion analysis using manifold ray casting of volumetrically fused multi-view range imaging.
  In Mori, K., Sakuma, I., Sato, Y., Barillot, C., and Navab, N., editors, *Medical Image Computing and Computer-Assisted Intervention MICCAI 2013*, Lecture Notes in Computer Science, pages 116–123. Springer.
- Williams, C. and Seeger, M. (2001).
  Using the nyström method to speed up kernel machines.
  In *Advances in Neural Information Processing Systems 13*, pages 682–688. MIT Press.

Related Work

[Fayad et al., 2012]	Heuristic partitioning of surface depth maps
[Hughes et al., 2009]	Simulate 1-D surrogates, e.g. the estimated lung volume
[Schaerer et al., 2012], [Bauer et al., 2012]	Actual surface motion tracking, but no internal prediction
[Klinder et al., 2010]	Generic prediction framework, not evaluated on surface surrogates
[He et al., 2010]	External fiducials, simulate respiratory phases from 3-D CT of unseen subject

Nonrigid Volumetric Registration Details

- Symmetric Demons forces:

$$\boldsymbol{v} = \frac{2(\boldsymbol{R} - \boldsymbol{T_D})(\nabla \boldsymbol{R} + \nabla \boldsymbol{T_D})}{\|\nabla \boldsymbol{R} + \nabla \boldsymbol{T_D}\|_2^2} \tag{8}$$

- Cf. derivative of SSD: $\boldsymbol{v} = 2(\boldsymbol{R} - \boldsymbol{T_D})\nabla \boldsymbol{T_D}$
- Curvature regularization:

$$\mathcal{S}^{\text{curv}}[\boldsymbol{D}] = \frac{1}{2}\sum_{\ell=1}^{d} \int_{\Omega} (\Delta \boldsymbol{D}_{\ell})^2 \mathrm{d}\boldsymbol{x} \tag{9}$$

- Gâteaux derivative of Eq. (9) is $\mathcal{A}^{\text{curv}}[\boldsymbol{D}] = \Delta^2 \boldsymbol{D}$

Internal Model Details

- For faster convergence, initialize optimization with result of nearest phase closer to reference
- Deformation fields are $2\times$ downsampled and cropped to internal ROI
- The $\tilde{\boldsymbol{d}}_t^{\text{int}}$ are few, but high-dimensional:

  Eigendecompose Gram matrix $\boldsymbol{K} = \boldsymbol{Y}\boldsymbol{Y}^\top$ instead of $\Sigma_{\boldsymbol{Y}} = \boldsymbol{Y}^\top\boldsymbol{Y}$

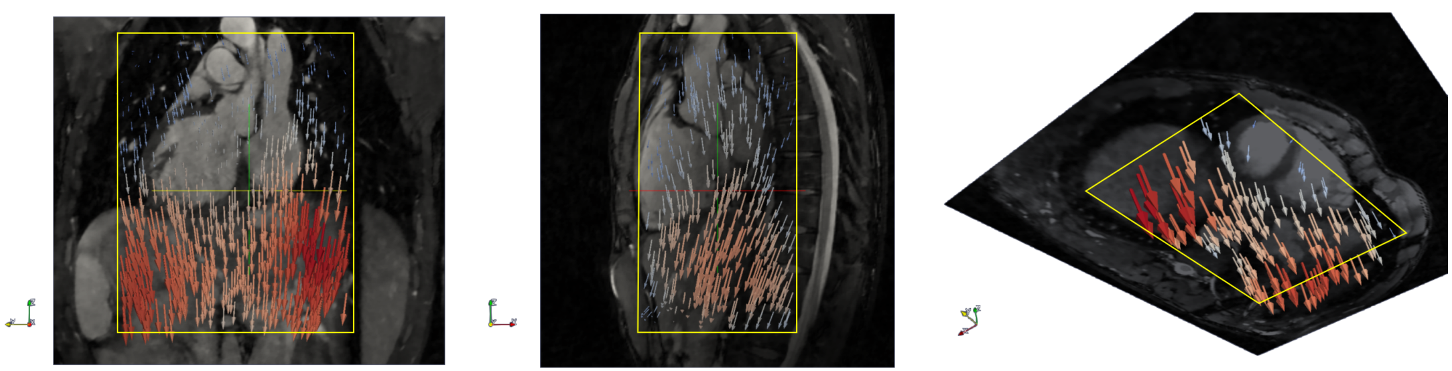

Surface Extraction (cont.)

- Find air-skin transition with heuristic thresholding
- Postprocessing (smoothing, closing holes) required due to fat saturation in cardiac MRI sequence
- Interpolate deformation fields at vertex positions to obtain motion

Figure: Extracted body surface before (left) and after (middle, right with motion vectors) postprocessing.

Multilinear Regression

- Closed form solution: $\boldsymbol{B} = \boldsymbol{Y}_m^\top \boldsymbol{X}_m \left(\boldsymbol{X}_m^\top \boldsymbol{X}_m\right)^{-1}$
- $\boldsymbol{X}_m \left(\boldsymbol{X}_m^\top \boldsymbol{X}_m\right)^{-1} = \left(\boldsymbol{X}_m^\top\right)^\dagger$ is the Moore-Penrose pseudoinverse.
- Tikhonov regularization / ridge regression: If numerically unstable,

$$\text{invert} \quad \boldsymbol{X}_m^\top \boldsymbol{X}_m + \gamma \boldsymbol{I} \quad \text{instead of} \quad \boldsymbol{X}_m^\top \boldsymbol{X}_m. \tag{10}$$

Internal Motion Prediction

- Elastic registration of instantaneous to reference surface
  - Nonrigid ICP variant [Schaerer et al., 2012]
  - Model-based ICP with 4-D shape priors [Wasza et al., 2012]
  - Active Laser Triangulation [Bauer et al., 2012]
- Out-of-sample extension of external model
  - Trivial for PCA: subtract mean and project onto eigenvectors
  - Approximate solution needed for kernel methods
    (Nyström method, [Williams and Seeger, 2001, Bengio et al., 2003])
- Perform regression, reconstruct with principal components

Internal Motion Prediction

- Elastic registration of instantaneous to reference surface
  - Nonrigid ICP variant [Schaerer et al., 2012]
  - Model-based ICP with 4-D shape priors [Wasza et al., 2012]
  - Active Laser Triangulation [Bauer et al., 2012]
- Out-of-sample extension of external model
  - Trivial for PCA: subtract mean and project onto eigenvectors
  - Approximate solution needed for kernel methods (Nyström method, [Williams and Seeger, 2001, Bengio et al., 2003])
- Perform regression, reconstruct with principal components

Internal Motion Prediction

- Elastic registration of instantaneous to reference surface
  - Nonrigid ICP variant [Schaerer et al., 2012]
  - Model-based ICP with 4-D shape priors [Wasza et al., 2012]
  - Active Laser Triangulation [Bauer et al., 2012]
- Out-of-sample extension of external model
  - Trivial for PCA: subtract mean and project onto eigenvectors
  - Approximate solution needed for kernel methods (Nyström method, [Williams and Seeger, 2001, Bengio et al., 2003])
- Perform regression, reconstruct with principal components

Data Sizes

ID	Phases	Size [voxels]	Spacing [mm]	Int. ROI [voxels]	Surface Vert.
P1	13	$256 \times 288 \times 256$	1.05	$110 \times 170 \times 200$	5,368
P2	18	$256 \times 320 \times 256$	1.00	$110 \times 190 \times 160$	4,321
P3	16	$352 \times 320 \times 352$	1.00	$90 \times 185 \times 200$	6,628
P4	13	$352 \times 320 \times 352$	1.00	$120 \times 195 \times 200$	3,759
P5	12	$256 \times 256 \times 256$	1.05	$85 \times 155 \times 180$	4,493
P6	8	$256 \times 144 \times 256$	1.05	$105 \times 125 \times 190$	2,521
XCAT	15	$256 \times 256 \times 256$	1.50	$70 \times 100 \times 125$	5,566

Default Method Parameters

- $l = r = 4$
- Kernel PCA, $\sigma = 40$ for MRI and $\sigma = 400$ for XCAT data
- Isomap, $k = 4$ ($k = 7$ if graph not fully connected)
- $\alpha = 2500$ (cf. Eq. (1)) and full surface coverage

Cumulative Relative Eigenvalues

For P1 with $\alpha = 2500$:

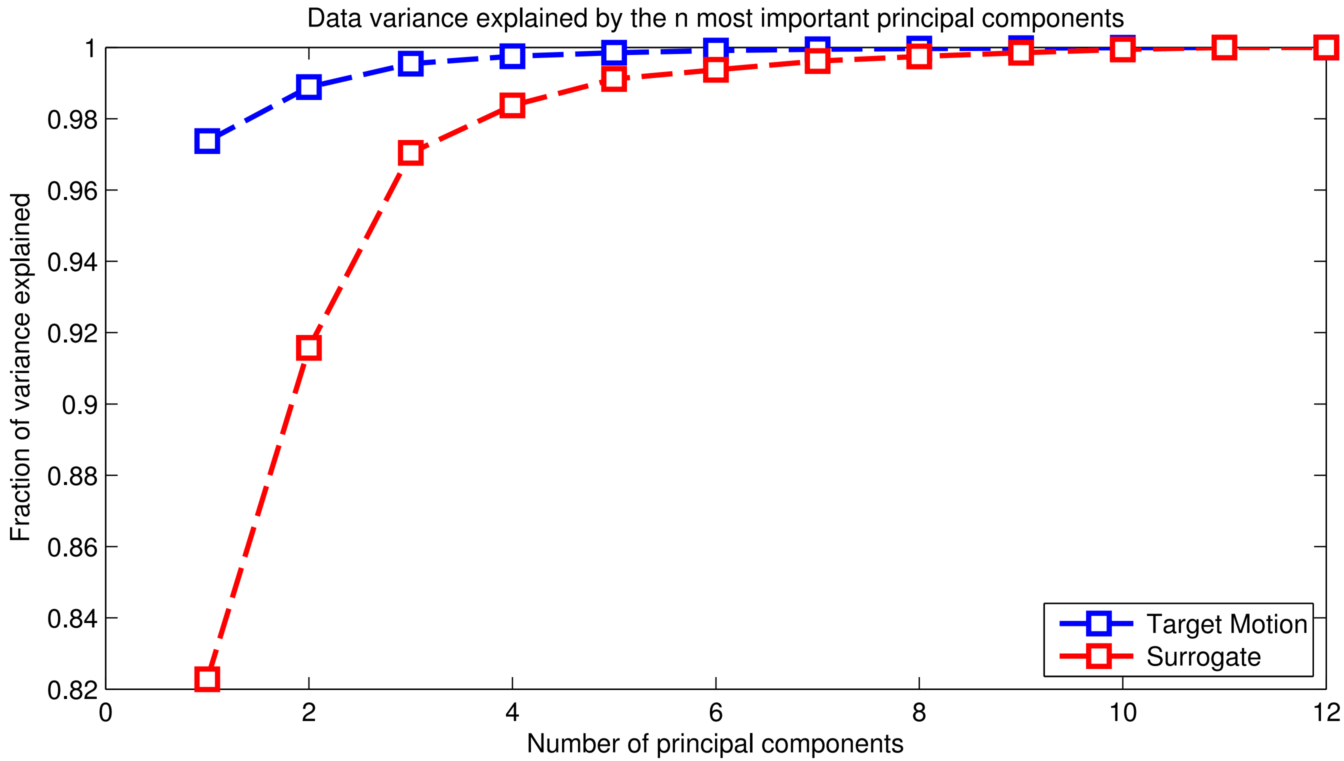

Cumulative Relative Eigenvalues

For P1 with $\alpha = 500$:

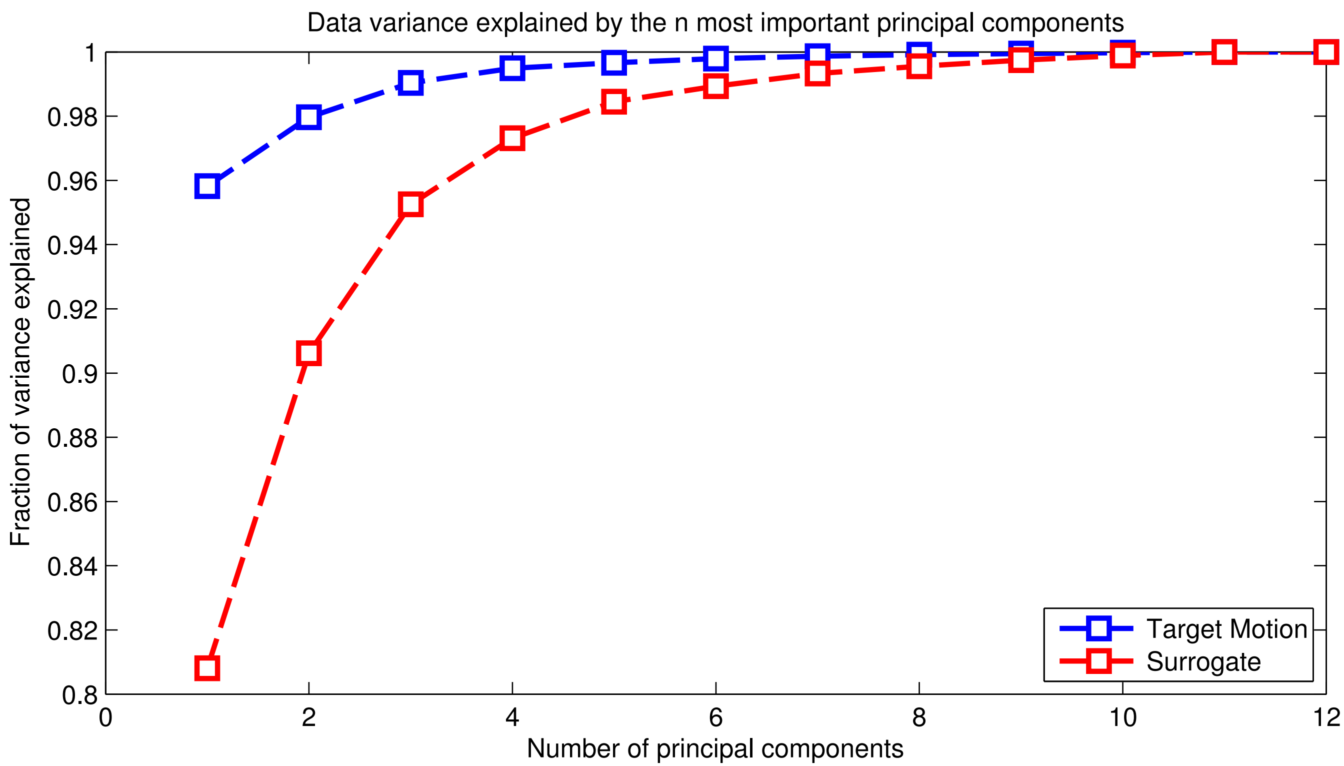

Cumulative Relative Eigenvalues

For P1 with $\alpha = 50$:

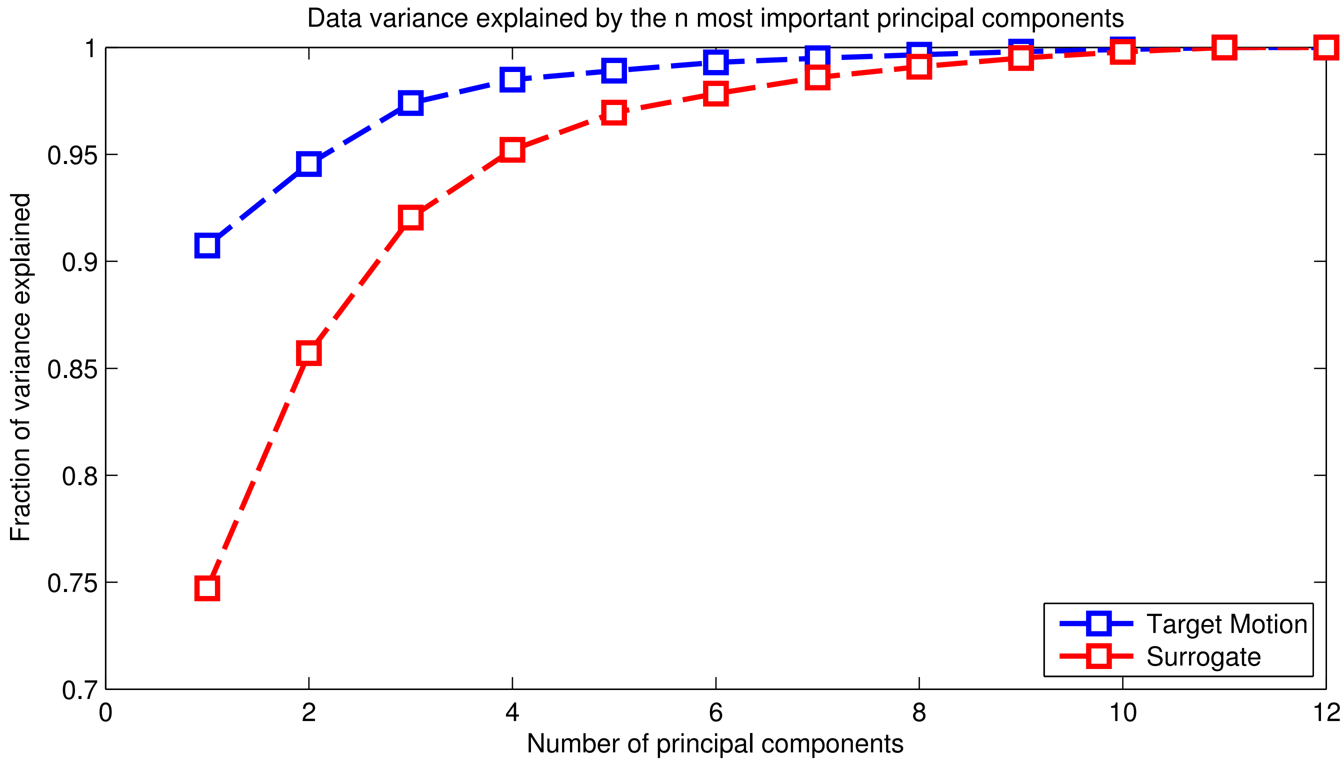

Errors – Dimensionality Reduction Options

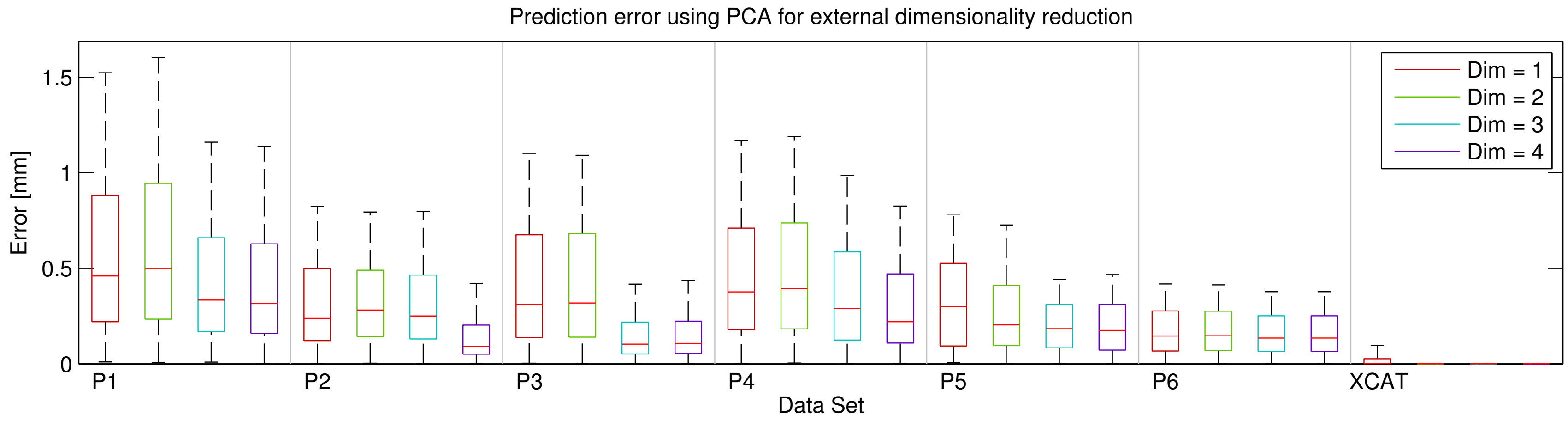

Errors – Dimensionality Reduction Options

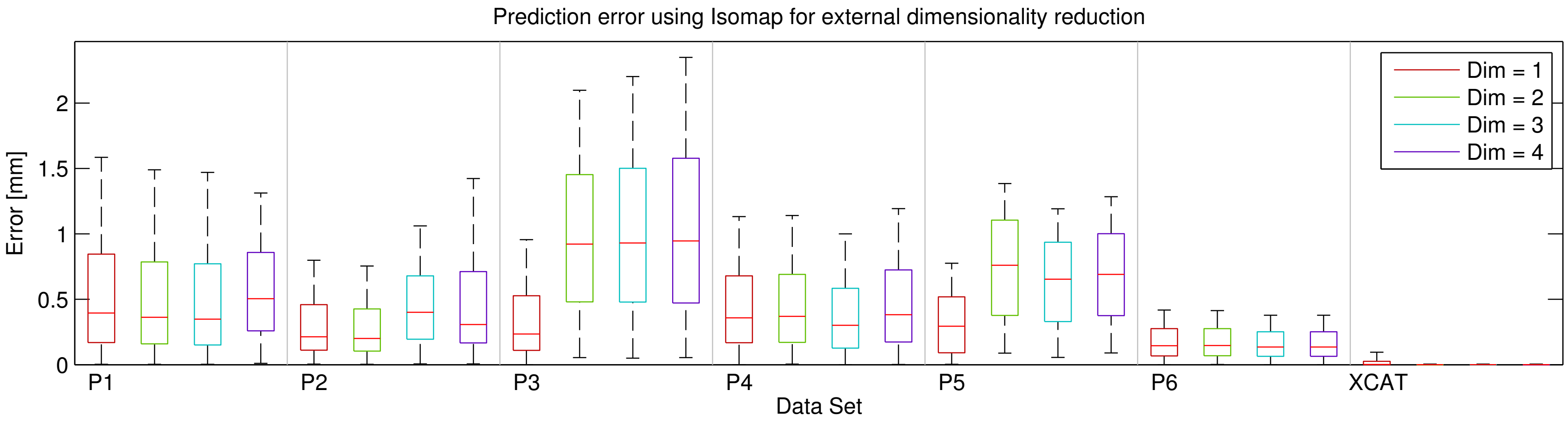

Errors – Dimensionality Reduction Options

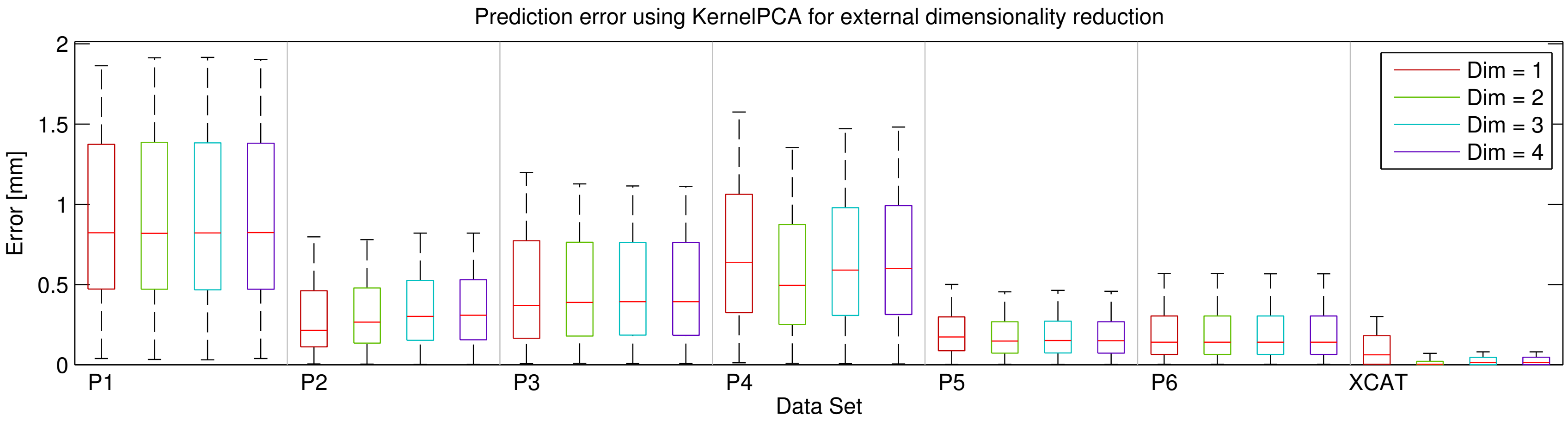

Results – Dimensionality Reduction Options

- PCA outperforms nonlinear methods w. r. t. prediction error, improves with increasing feature space dimensionality
- Isomap and Kernel PCA not quite as accurate, only most significant feature dimension is meaningful
- Best result in MRI: max. error of 0.42 mm, given a median magnitude of 3.91 mm in the ground truth deformation field
- Phantom is predicted almost perfectly in any configuration

Results – Runtimes

- Training phase (not time-critical):
  - Registration (C++, using ITK): $\approx$ one to several hours for a whole sequence
  - Surface extraction (C++, using RITK): $\approx$ few ms (+ manual param. choice)
  - Mesh processing (ParaView, Meshlab): $\approx$ few minutes (automatic + manual)
  - Model training (MATLAB, using DR toolbox): $\approx$ few seconds
- Application phase (usually time-critical):
  - Deformable mesh registration: e.g. $\approx$ 40 ms on GPU with [Wasza et al., 2013] (untested as no RI data were used in our experiments)
  - Prediction using PCA for both models (CUDA, using cuBLAS): 5-10 ms

Results – Runtimes

- Training phase (not time-critical):
  - Registration (C++, using ITK): $\approx$ one to several hours for a whole sequence
  - Surface extraction (C++, using RITK): $\approx$ few ms (+ manual param. choice)
  - Mesh processing (ParaView, Meshlab): $\approx$ few minutes (automatic + manual)
  - Model training (MATLAB, using DR toolbox): $\approx$ few seconds
- Application phase (usually time-critical):
  - Deformable mesh registration: e.g. $\approx$ 40 ms on GPU with [Wasza et al., 2013] (untested as no RI data were used in our experiments)
  - Prediction using PCA for both models (CUDA, using cuBLAS): 5-10 ms